Structural Engineering and Mechanics, *Vol. 71, No. 6 (2019) 699-712*
DOI: https://doi.org/10.12989/sem.2019.71.6.699

Hydro-mechanical interaction of reinforced concrete lining in hydraulic pressure tunnel

He-Gao Wu[1a], Li Zhou[1b], Kai Su*[1], Ya-Feng Zhou[2c] and Xi-Yu Wen[3d]

[1]*State Key Laboratory of Water Resources and Hydropower Engineering Science, Wuhan University, 430072 Wuhan, China*
[2]*Changjiang Institute of Survey, Planning, Design and Research, 430010 Wuhan, China*
[3]*Changjiang Geotechnical Engineering Corporation, 430010 Wuhan, China*

(Received November 1, 2018, Revised April 19, 2019, Accepted April 24, 2019)

Abstract. The reinforced concrete lining of hydraulic pressure tunnels tends to crack under high inner water pressure (IWP), which results in the inner water exosmosis along cracks and involves typical hydro-mechanical interaction. This study aims at the development, validation and application of an indirect-coupled method to simulate the lining cracking process. Based on the concrete damage plasticity (CDP) model, the utility routine GETVRM and the user subroutine USDFLD in the finite element code ABAQUS is employed to calculate and adjust the secondary hydraulic conductivity according to the material damage and the plastic volume strain. The friction-contact method (FCM) is introduced to track the lining-rock interface behavior. Compared with the traditional node-shared method (NSM) model, the FCM model is more feasible to simulate the lining cracking process. The number of cracks and the reinforcement stress can be significantly reduced, which matches well with the observed results in engineering practices. Moreover, the damage evolution of reinforced concrete lining can be effectively slowed down. This numerical method provides an insight into the cracking process of reinforced concrete lining in hydraulic pressure tunnels.

Keywords: hydraulic pressure tunnel; reinforced concrete lining; hydro-mechanical interaction; crack; indirect-coupled method; friction-contact method

1. Introduction

Along with the rapid development of global low-carbon economy and engineering technology, the underground hydraulic pressure tunnels with reinforced concrete lining have been more and more applied in pumped storage power stations and water conservancy projects. Compared with the steel liner, which is waterproof but expensive and inconvenient for construction, the reinforced concrete lining has the advantage of saving the construction period, and it is feasible to make cracks and inner water exosmosis under control with the pre-embedded reinforcements (Zhou *et al.* 2015). The employment of reinforced concrete lining can effectively reduce the head loss and improve the anti-permeability of surrounding rock, in addition to protecting the rock mass against erosion and destruction from high-velocity water flows (Bian *et al.* 2016, Jaeger 1979).

The reinforced concrete lining in hydraulic pressure tunnels tends to crack under high inner water pressure (IWP), subsequently resulting in the inner water exosmosis. Longitudinal cracks lead to major changes in the material properties of cracked concrete, including the permeability and the constitutive relationship. The lining cracking process shows typical hydro-mechanical coupling characteristics, which contains the following two aspects (Schleiss 1986): hydraulic mechanics and structural mechanics. The hydraulic mechanics problem refers to the seepage calculation with the secondary material permeability induced by structural stress state. While the structural mechanics problem is based on the structural analysis of stress and deformation under the impact of seepage body force obtained from the seepage calculation. The seepage field interacts with the stress field until a new equilibrium between hydraulic and mechanical iterations is achieved.

The investigation of hydro-mechanical interaction during the lining cracking process has attracted lots of researchers and some achievements have been made in the past few decades. Schleiss (1986) pointed out the deficiencies of traditional pressure tunnel statics and introduced the hydro-mechanical interaction into the theoretical computation of pervious pressure tunnels, which laid the foundation for this issue. Based on this, Schleiss (1997) discussed the design criterion of reinforced concrete lined pressure tunnels, and found that the crack width on the lining concrete, which affects the hydro-mechanical coupling behaviors, is closely related to the specification and arrangement of embedded reinforcements. Yoo (2005) presented a 3D stress-pore pressure coupled finite element method to investigate the interaction between tunneling and groundwater, and found that the lining responses are significantly affected by its relative permeability. Shin (2008) and Yoon *et al.* (2014) investigated the coupled

*Corresponding author, Professor
E-mail: ksu@whu.edu.cn
[a] Ph.D. Professor
[b] Ph.D. Candidate
[c] Senior Engineer
[d] Engineer

http://www.techno-press.com/journals/sem&subpage=7
ISSN: 1225-4568 (Print), 1598-6217 (Online)

hydro-mechanical behaviors of lining by a combination of beam and solid elements. The lining distortions, forces and moments can be directly obtained with this method. Based on the plane strain axisymmetric assumption, Fahimifar and Zareifard (2009) proposed an analytical unclosed form solution to the pressure tunnel below the groundwater table. The necessity of considering the coupled hydraulic and mechanical effects of a pervious lining was demonstrated through contrastive analysis. Bian *et al.* (2009) applied the proposed hydro-mechanical coupling method to the structural analysis of reinforced concrete lined underground pipe under IWP. It was found that the maximum tensile stress of lining can be effectively reduced with the increase of reinforcement ratio, and the crack roughness only affects the permeability of cracked concrete, but has little influence on the lining stress. Graziani and Boldini (2012) investigated the influence of hydro-mechanical interaction on the tunnel responses and pointed out that the coupled analysis is necessary because the uncoupled analysis underestimates the long-term load on the pervious lining. Olumide and Marence (2012) and Olumide (2013) analyzed the hydro-mechanical interaction during the cracking process of plain concrete lining by the superposition of consolidation and seepage analyses. It was found that the prestressing of surrounding rock by grouting can effectively limit the inner water exosmosis within an acceptable range. In order to estimate the distribution of seepage water pressure and the inner water leakage, Simanjuntak *et al.* (2013) studied the mechanical-hydraulic interaction in the lining cracking process and confirmed the relevance of seepage pressures on the bearing capacity of pressure tunnels. Zhou *et al.* (2015) pointed out the nonuniform strains of reinforcements and concrete after the lining cracking, and introduced the nonuniformity coefficients to reflect this characteristic. Based on this, an equivalent hydro-mechanical coupling method was proposed to simulate the lining cracking process. Zareifard and Fahimifar (2016) proposed an analytical solution to estimate the structural responses induced by seepage flows and concluded that the classic Lame's solution results in unreliable tunnel design. Xiao and Zhao (2017) developed a hydro-mechanical coupling model for the cracking of reinforced concrete lining by changing the structural plastic stiffness, and the influence of inner water exosmosis on collapse was investigated. Dadashi *et al.* (2017, 2018) adopted a direct-coupled method to simulate the hydro-mechanical interaction and found that an appropriate distribution of embedded reinforcements can effectively minimize the inner water leakage. The lining cracking could be controlled by the optimization of reinforcement distribution and lining thickness. Zareifard (2018) systematically summarized the design methods of hydraulic pressure tunnel and implemented the hydro-mechanical coupling analysis by an iterative procedure, which provides some guidance for the design and construction of pressure tunnels. However, most of the abovementioned research achievements cannot properly explain such an engineering phenomenon that the reinforcement stress in the actual operation period of pressure tunnels is far lower than expected. For example, the tensile reinforcement stress increased with the IWP only at the early stage of water-filling period in Guangzhou Pumped Storage Power Station. The increment of reinforcement stress slowed down significantly after the lining cracking, and even there is a tendency of stress retraction. The maximum reinforcement stress was only 49.5MPa when the IWP reached 6.1MPa. A similar phenomenon also occurred in Zhouning Hydropower Station and the reinforcement stress ranged from 0 to 50MPa (Zhou *et al.* 2015).

The hydro-mechanical interaction of reinforced concrete lining in hydraulic pressure tunnels is generally analyzed under the assumption that the lining and the surrounding rock are well-combined during the whole water-filling process. Therefore, the traditional node-shared method (NSM) is often employed to simulate the lining-rock interface, in which the lining and the surrounding rock are connected by sharing nodes at their interface. Even if not, the lining and the surrounding rock are assumed to be tied together without relative displacement (Lyu *et al.* 2018). Many cracks can be found on the reinforced concrete lining when the traditional NSM models are utilized (Bian *et al.* 2009). However, only a few cracks were present in several large-scale water-filling engineering tests (Zhou *et al.* 2018). This disagreement between the numerical results in the NSM models and the experimental data cannot be effectively addressed, and it is always ignored by most researchers.

In fact, the reinforced concrete lining might be detached from the surrounding rock during the water-filling process, and the stress distribution of hydraulic pressure tunnel will be significantly affected by the coupled hydraulic and structural lining-rock interaction (Leung and Meguid 2011, Shin 2008, Shin *et al.* 2012). Before the lining cracking, the displacement continuity and flow continuity conditions are satisfied at the lining-rock interface (Zhou *et al.* 2015). The seepage water pressure on the lining extrados is rather low and the lining bears most of the water load since the fact that the permeability of the integral lining concrete is much weaker than that of the surrounding rock. As the IWP increases, the lining cracks and consequently its permeability is greatly improved by several orders of magnitude (Picandet *et al.* 2009). The inner water flows off along cracks, resulting in a great decline of the hydraulic gradient inside the lining. Correspondingly the surrounding rock becomes the main object to bear the water load and greater outward deformation will be induced. However, the outward deformation of lining is obviously weakened due to the significant decline of hydraulic gradient and the constraints of embedded reinforcements. A tensile stress will arise at the lining-rock interface when the outward deformation of surrounding rock is larger than that of lining, and a gap will appear once the tensile stress exceeds the tensile strength of lining-rock interface (Bobet and Nam 2007, Fernández 1994). This mechanism has been validated from the perspective of analytical solution, and the critical conditions for the detachment between lining and surrounding rock have been derived on the basis of thick-walled cylinder model (Fernández 1994, Schleiss 1986, 1997). In aspect of numerical simulation, Zhou *et al.* (2015) adopted the water-filled joint (WFJ) elements to model the lining-rock interface, the mechanics and hydraulic characteristics of the interface could be reflected by the material strength and hydraulic conductivity of WFJ elements. In engineering practice, gap gauges were embedded at the top, waist and bottom positions of lining extrados during the water-filling test of hydraulic pressure tunnel in Tianhuangping Pumped Storage Power Station, and the observed data intuitively indicated that detachments had appeared at these three monitoring positions (Hou 2009).

In this study, an indirect-coupled method is developed to analyze the hydro-mechanical interaction of reinforced concrete lining in hydraulic pressure tunnels based on the concrete damage plastic (CDP) model. The secondary hydraulic conductivity is evaluated according to the material damage and the plastic volume strain with the adoption of utility routine GETVRM and user subroutine USDFLD in the finite element code ABAQUS. Hence, a seepage-stress-damage coupling model of hydraulic pressure tunnel is developed, in which the node-shared method (NSM) and the friction-contact method (FCM) are utilized to simulate the lining-rock interface respectively.

2. Theoretical model of structure

2.1 Concrete damage plasticity (CDP) model

Based on the continuum damage mechanics framework, the discontinuous macro-crack brittle behaviors on the lining concrete are realized by the concrete damage plasticity (CDP) model. In the CDP model, a single macro-crack is implicit and not traced. The mechanical effects of cracks are reflected by the structural stiffness degradation related to the material damage (Su *et al*. 2017). Therefore, the geometry and width of cracks cannot be computed directly in the numerical simulation (Dadashi *et al*. 2017). In the previous research work, the CDP model has been widely adopted in the nonlinear numerical analysis of structures composed of concrete or other quasi-brittle materials, and it can effectively reflect the lining cracking process in hydraulic pressure tunnels (Dadashi *et al*. 2017, Grassl and Jirásek 2006, Su *et al*. 2017, Zhou *et al*. 2018). Rama *et al*. (2017) conducted a parametric study of CDP model and found that the cracking characteristics of concrete for different grades can be adequately predicted without indoor tests.

The CDP model, whose yield criterion was proposed by Lubliner *et al*. (1989) and amended by Lee and Fenves (1998), is utilized to model the lining concrete within the finite element code ABAQUS. The constitutive relationship of this model is intended to track the influences of the irreversible concrete damage linked to the failure mechanism on the structural nonlinear behaviors, and it plays the key role to reflect the mechanical responses and failure mechanism of concrete (Lyu *et al*. 2018). The concrete damage d is a scalar and it will lead to the isotropic elastic stiffness degradation (Cicekli *et al*. 2007, Grassl and Jirásek 2006, Jankowiak and Lodygowski 2005, Lubliner *et al*. 1989). Under the three-dimensional multiaxial condition, the stress-strain relationship can be expressed as follows

$$\sigma = (1-d)D_0^{el} : (\varepsilon - \varepsilon^{pl}) = D^{el} : (\varepsilon - \varepsilon^{pl}) \tag{1}$$

where σ refers to the concrete stress, D_0^{el} is the initial (undamaged) elastic stiffness, the degraded stiffness $D^{el} = (1-d)D_0^{el}$, ε represents the concrete strain and the ε^{pl} denotes the plastic strain.

The concrete effective stress $\bar{\sigma}$ can be calculated based on Eq. (2).

$$\bar{\sigma} \overset{def}{=} D_0^{el} : (\varepsilon - \varepsilon^{pl}) \tag{2}$$

The concrete damage is related to the equivalent plastic strain $\tilde{\varepsilon}^{pl}$, which can be expressed as follows

$$\tilde{\varepsilon}^{pl} = \begin{bmatrix} \tilde{\varepsilon}_t^{pl} \\ \tilde{\varepsilon}_c^{pl} \end{bmatrix} = \begin{bmatrix} \int_0^t \dot{\tilde{\varepsilon}}_t^{pl} dt \\ \int_0^t \dot{\tilde{\varepsilon}}_c^{pl} dt \end{bmatrix}; \dot{\tilde{\varepsilon}}^{pl} = \begin{bmatrix} \dot{\tilde{\varepsilon}}_t^{pl} \\ \dot{\tilde{\varepsilon}}_c^{pl} \end{bmatrix} = \hat{h}\left(\hat{\bar{\sigma}}, \tilde{\varepsilon}^{pl}\right) \cdot \hat{\dot{\varepsilon}}^{pl} \tag{3}$$

where t and c refer to tensile and compressive states, $\dot{\tilde{\varepsilon}}^{pl}$ and $\hat{\dot{\varepsilon}}^{pl}$ denote the equivalent plastic strain rate and the eigenvalue of plastic strain rate tensor respectively, $\hat{h}\left(\hat{\bar{\sigma}}, \tilde{\varepsilon}^{pl}\right)$ can be expressed as Eq. (4).

$$\hat{h}\left(\hat{\bar{\sigma}}, \tilde{\varepsilon}^{pl}\right) = \begin{bmatrix} r\left(\hat{\bar{\sigma}}\right) & 0 & 0 \\ 0 & 0 & -\left(1 - r\left(\hat{\bar{\sigma}}\right)\right) \end{bmatrix} \tag{4}$$

The multiaxial stress weight factor $r\left(\hat{\bar{\sigma}}\right)$ is evaluated according to Eq. (5).

$$r\left(\hat{\bar{\sigma}}\right) \overset{def}{=} \frac{\sum_{i=1}^{3} \left\langle \hat{\bar{\sigma}}_i \right\rangle}{\sum_{i=1}^{3} \left| \hat{\bar{\sigma}}_i \right|}; 0 \le r\left(\hat{\bar{\sigma}}\right) \le 1 \tag{5}$$

where $\hat{\bar{\sigma}}_i (i = 1,2,3)$ refers to the principal stresses and $\langle x \rangle = 0.5(|x| + x)$.

The plastic strain rate $\dot{\varepsilon}^{pl}$ is controlled by the nonassociated flow rule, which is related to the flow potential G.

$$\dot{\varepsilon}^{pl} = \dot{\lambda} \frac{\partial G(\bar{\sigma})}{\partial \bar{\sigma}}; G = \sqrt{(\varsigma \sigma_{t0} \tan\psi)^2 + \bar{q}^2} - \bar{p} \tan\psi \tag{6}$$

where $\dot{\lambda}$ refers to a nonnegative multiplier, ς represents the eccentricity, σ_{t0} denotes the tensile failure stress, ψ refers to the dilation angle, the effective hydrostatic pressure $\bar{p} = -\frac{1}{3}\bar{\sigma} : I$, the effective hydrostatic pressure $\bar{q} = \sqrt{\frac{3}{2}\bar{S} : \bar{S}}$, and $\bar{S} = \bar{p}I + \bar{\sigma}$.

The focus of this study is on the tensile cracking of reinforced concrete lining considering its mechanical responses under the IWP and the fact that the compressive strength of concrete is generally high, although the CDP model assumes that the tensile cracking and compressive crushing are the main two failure mechanisms (ABAQUS 2011). When the CDP model is defined in ABAQUS, the σ_t - ε_t^{pl} relationship and d_t - ε_t^{pl} relationship that need to be predefined are obtained under the uniaxial condition. The conversion from uniaxial condition to multiaxial condition is performed automatically by ABAQUS. Under the uniaxial condition, σ_t and d_t can be defined by the following comprehensive functions.

$$\sigma_t = \sigma_t(\tilde{\varepsilon}_t^{pl}, \dot{\varepsilon}_t^{pl}, \theta, f_i) \tag{7}$$

$$d_t = d_t(\tilde{\varepsilon}_t^{pl}, \theta, f_i), (0 \le d_t \le 1) \tag{8}$$

where θ denotes the temperature and $f_i (i = 1,2\ldots)$ refer to other field variables.

In this study, the following concrete stress-strain formula provided by the Code for Design of Concrete Structures from the People's Republic of China (No. GB 50010-2010) (MOHURD 2010) is adopted, and it is assumed that σ_t is independent of θ and f_i.

$$\sigma_t = \frac{f_t^*}{\dfrac{\alpha_t f_t^*}{E_0 \varepsilon_t}\left(\dfrac{E_0 \varepsilon_t}{f_t^*} - 1\right)^{1.7} + 1} \tag{9}$$

where $\alpha_t = 0.31 f_t^{*2}$, f_t^* refers to the tensile strength; ε_t represents the total tensile strain and E_0 denotes the elastic modulus.

The tensile damage of concrete is determined according to the continuum damage theory (Mazars and Pijaudier Cabot 1989), and it is assumed that d_t is independent of θ and f_i. The tensile damage-strain formula can be expressed as Eq. (10).

$$d_t = 1 - \frac{\varepsilon_t^*(1 - A_t)}{\varepsilon_t} - \frac{A_t}{\exp[B_t(\varepsilon_t - \varepsilon_t^*)]} \tag{10}$$

where A_t and B_t are the parameters related to the uniaxial tensile test, the critical total strain when damage initiates $\varepsilon_t^* = f_t^* / E_0$.

In this study, the lining is considered to be made of concrete C25. Based on the research work of Su *et al*. (2017), f_t^* =1.27MPa, E_0 =28GPa, $A_t = 0.68$ and $B_t = 10^4$ are used. The reliability of these parameters has been verified because the calculated cracking characteristics of surrounding reinforced concrete in penstock matched well with the observed results of Li-Jia-Xia Hydropower Station. The plastic strain can be calculated as $\varepsilon^{pl} = \varepsilon_t - \varepsilon_t^*$. Therefore, the σ_t - ε_t^{pl} and d_t - ε_t^{pl} relationships have been completed and can be illustrated as Fig.1.

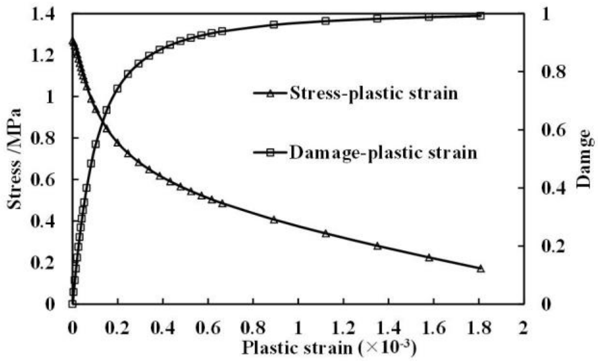

Fig. 1 Evolution curves of tensile stress and damage

2.2 Modeling of embedded reinforcements

For the reinforcement stress-strain relationship obtained by indoor tensile test, after some reasonable and ideal simplifications, the reinforcement stress-strain models used for structural analysis can be obtained. Among these constitutive models, the linear elastic and perfectly plastic model is frequently employed to simulate the metal elastic-plastic behaviors, although it ignores the strain-hardening effects of reinforcements. This constitutive relationship can be presented as Eq. (11).

$$\begin{cases} \sigma_s = E_s \varepsilon_s & , \quad \varepsilon_s < f_y / E_s \\ \sigma_s = f_y & , \quad \varepsilon_s \ge f_y / E_s \end{cases} \tag{11}$$

where ε_s refers to the reinforcement strain, and f_y is the metal yield stress.

In this study, the reinforcement elements are assumed to be fully embedded in the solid concrete elements without sliding and superposed on the mesh of concrete elements (ABAQUS 2011). Therefore, the cracking of reinforced concrete lining is simulated by the CDP model with the embedded reinforcements. Within continuum damage mechanics framework, the concrete cracks are not discrete but equivalent continuous. The cracked concrete is characterized with a postfailure strain-softening behavior and in a low stress state, while the integral tensile concrete located in the uncracked zones maintains the load capacity. The seepage loads are still shared by the concrete and embedded reinforcements, which reflect the tension-stiffening effect of cracked reinforced concrete structures (Zareifard 2018).

2.3 Modeling of surrounding rock

The surrounding rock is simplified to linear elastic since the focus of this study is on the cracking process of reinforced concrete lining and the resulting hydro-mechanical coupling characteristics (Zhang *et al*. 2018). This simplification can be found in some research work of previous studies, such as Fahimifar and Zareifard (2013), Fernández (1994), Schleiss (1986, 1997), Simanjuntak *et al*. (2013), Zareifard (2018), Zareifard and Fahimifar (2016), Zhang *et al*. (2018) and so on. These references indicate this simplification can work in principle, although it may not account for the reality of surrounding rock accurately. In addition, the simplification of surrounding rock can improve the convergence stability of serious nonlinear analysis. This simplification is feasible as long as the calculated results of reinforced concrete lining are within the acceptable errors. The stress-strain relationship can be expressed as Eq. (12).

$$\begin{Bmatrix} \varepsilon_{11} \\ \varepsilon_{22} \\ \varepsilon_{33} \\ \gamma_{12} \\ \gamma_{13} \\ \gamma_{23} \end{Bmatrix} = \begin{bmatrix} 1/E & -\nu/E & -\nu/E & 0 & 0 & 0 \\ -\nu/E & 1/E & -\nu/E & 0 & 0 & 0 \\ -\nu/E & -\nu/E & 1/E & 0 & 0 & 0 \\ 0 & 0 & 0 & 1/G & 0 & 0 \\ 0 & 0 & 0 & 0 & 1/G & 0 \\ 0 & 0 & 0 & 0 & 0 & 1/G \end{bmatrix} \begin{Bmatrix} \sigma_{11} \\ \sigma_{22} \\ \sigma_{33} \\ \tau_{12} \\ \tau_{13} \\ \tau_{23} \end{Bmatrix} \quad (12)$$

where E denotes the elastic modulus, ν represents the Poisson's ratio and $G = E/2(1+\nu)$.

3. Hydro-mechanical interaction

3.1 Indirect-coupled method

The direct-coupled method and the indirect-coupled method are the main two prevailing coupling method of hydro-mechanical interaction (Zhou *et al.* 2015). In the direct-coupled method, the hydraulic mechanics and the structural mechanics are solved synchronously with a coupled equation. However, some theoretical and numerical challenges need to be faced when simulating the coupling behaviors with this method. In the indirect-coupled method, the abovementioned two aspects are evaluated in separate computation step, the coupling iterations between them continue until reaching an equilibrium state. To be specific, the seepage field affects the stress field through the equivalent node load generated by the seepage body force, while the stress field in turn exerts effects on the seepage field by the means of influencing the material permeability. During the iterative process, a coupled relationship between material permeability and structural stress state needs to be established.

In this study, the indirect-coupled method is adopted to analyze the hydro-mechanical interaction of reinforced concrete lining during its cracking process. The concrete damage represents the initiation and propagation of cracks, which leads to changes in the permeability of lining concrete (Xue *et al.* 2019). Therefore, the material damage and the plastic volume strain are introduced to quantifying the permeability evolution. The lining concrete belongs to one kind of pervious quasi-brittle material, and there is little change in its permeability before cracking. Once cracks appear, the hydraulic conductivity at the cracked sites will experience a sharp rise. Therefore, the jump factor ξ is introduced to evaluate the hydraulic effects of material damage d . The material element is composed of the damaged part and the undamaged part, and the hydraulic conductivity of the material element can be calculated as Eq. (13) (Zhou *et al.* 2018).

$$k(d, \varepsilon_v^p) = (1-d)k_m + dk_d(1+\varepsilon_v^{pf})^3 \quad (13)$$

where k_m is the hydraulic conductivity of the undamaged part, the plastic volume strain of damaged part $\varepsilon_v^{pf} = d\varepsilon_v^p$, and ε_v^p denotes the element plastic volume strain, the hydraulic conductivity of the damaged part $k_d = \xi k_m$, and ξ can be estimated according to Eq. (14).

$$\xi = \begin{cases} 10, & 0 < d \le 0.1 \\ \dfrac{1000-10}{0.9-0.1} d + 10, & 0.1 < d < 0.9 \\ 1000, & 0.9 \le d \le 1 \end{cases} \quad (14)$$

3.2 Iterative computation process

The seepage field is calculated under the assumption that the water and materials are incompressible, and the matrix equation of seepage field after the discretization of computational domain can be expressed as Eq. (15).

$$[K_s]\{h\} = \{A\} \quad (15)$$

where $[K_s]$ refers to the seepage matrix, $\{h\}$ denotes the node head column vector, $\{A\}$ represents the node load obtained by integrating the seepage boundary.

The equivalent node load $\{F_s\}$ can be estimated with Eq. (16) based on the seepage calculation.

$$\{F_s\} = -\iiint_\Omega \gamma [\mathbf{N}]^\mathrm{T} \left\{ \frac{\partial h}{\partial x}, \frac{\partial h}{\partial y}, \frac{\partial h}{\partial z} - 1 \right\}^T d\Omega \quad (16)$$

Under the node loads from structure and seepage, the stress field can be calculated with Eq. (17).

$$[K_m]\{u\} = \{F\} + \{F_s\} \quad (17)$$

where $[K_m]$ refers to the structural stiffness matrix, $\{u\}$ denotes the displacement column vector, and $\{F\}$ represents the node load from the structure.

The iterative computation between hydraulic mechanics and structural mechanics can be developed as: (ⅰ) $\{h\}$ is evaluated based on Eq. (15), and $\{F_s\}$ can be obtained with Eq. (16); (ⅱ) $\{u\}$ can be achieved according to Eq. (17); (ⅲ) the secondary $[K_s]$ is estimated by Eq. (13) and Eq. (14); (ⅳ) repeat steps (ⅰ)-(ⅲ) until reaching a new equilibrium.

4. Simulation of lining-rock interface

4.1 Lining-rock interface behavior

Fig. 2 illustrates the theoretical model of circular hydraulic pressure tunnel. The lining and the surrounding rock are treated as porous, homogeneous and pervious media. Before the lining cracking, the low-permeability of lining concrete indicates that the lining bears most of the water load, and the seepage water pressure is assumed to be

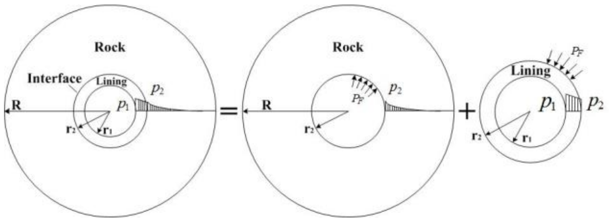

Fig. 2 Theoretical model of hydraulic pressure tunnel

logarithmic distributed (Schleiss 1986). The seepage water pressure p at arbitrary point can be estimated as follows

$$\begin{cases} p = \dfrac{p_1(\ln r_2 - \ln r) + p_2(\ln r - \ln r_1)}{\ln r_2 - \ln r_1} \\ \dfrac{dp}{dr} = \dfrac{1}{r} \cdot \dfrac{p_2 - p_1}{\ln r_2 - \ln r_1} \end{cases} \tag{18}$$

where p_1 and p_2 refer to the seepage water pressures on the lining intrados and extrados respectively, r_1 and r_2 denote the inner and outer radii, r is the distance between the tunnel center and the measured point.

In such case, the lining and the surrounding rock are well-combined. The displacement continuity and flow continuity conditions are satisfied at the lining-rock interface. Under the assumption that the hydraulic radius $R >> r_2$, the mechanical boundary load at the lining-rock interface P_F can be calculated by Eq. (19) (Schleiss 1986, 1997). Considering the fact that the hydraulic conductivity of integral concrete k_c is generally much smaller than that of surrounding rock k_r, P_F is compressive (P_F >0 represents compression).

$$\begin{cases} P_F = \dfrac{C_2 C_4 p_1 - (C_1 + C_2 C_4) p_2}{C_1 + C_2 C_3} \\ p_2 = \dfrac{k_c \ln(R / r_2)}{k_r \ln t + k_c \ln(R / r_2)} p_1 \end{cases} \tag{19}$$

where $C_1 = \dfrac{1+\mu_r}{E_r}$, $C_2 = \dfrac{1+\mu_c}{E_c}$, $C_3 = 1 - 2\mu_{c+} \dfrac{2-2\mu_c}{t^2-1}$, $C_4 = \dfrac{1-2\mu_c}{2\ln t} + \dfrac{1}{t^2-1}$, $t = r_2 / r_1$. μ_r and μ_c are the Poisson's ratios of rock mass and lining, E_r and E_c represent their elastic moduli respectively.

With the increment of IWP, the lining concrete cracks once the hoop tensile stress exceeds its tensile strength. The permeability of lining is greatly improved, and consequently the water load is mainly borne by the surrounding rock. The seepage water pressure inside the lining no longer meets the logarithmic distribution but the linear distribution (Schleiss 1986), and p inside the lining can be estimated as Eq. (20).

$$\begin{cases} p = \dfrac{p_1(r_2 - r) + p_2(r - r_1)}{r_2 - r_1} \\ \dfrac{dp}{dr} = \dfrac{p_2 - p_1}{r_2 - r_1} \end{cases} \tag{20}$$

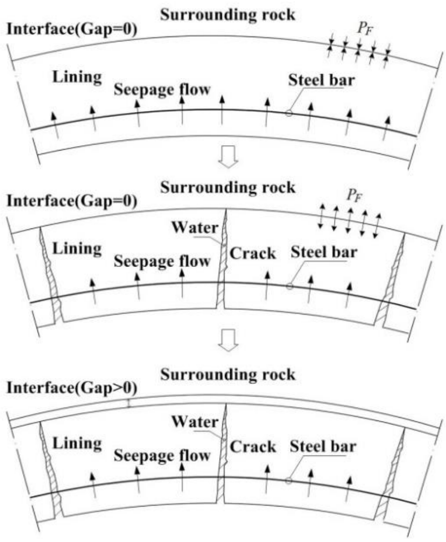

Fig. 3 Conceptual representation of lining-rock interface behavior

Under the assumption that the lining was still tightly attached to the surrounding rock after the lining cracking, P_F can be expressed as Eq. (21).

$$P_F = \frac{C_2 C_5 - (C_1 + C_2 C_5) C_6}{C_1 + C_2 C_3} p_1 \tag{21}$$

where $C_5 = \dfrac{2}{3}(\dfrac{2-\mu_c}{t^2-1}) + \dfrac{1-2\mu_c}{3(1-1/t)}$, and C_6 denotes the ratio of the seepage water pressure on the lining extrados to that on the lining intrados.

The outward deformation of surrounding rock is greater than that of lining after the lining cracking since the surrounding rock bears the most of the water load, and consequently P_F will be tensile (P_F <0 represents tension). Once $-P_F$ exceeds the tensile strength of lining-rock interface f_c, the detachment between lining and surrounding rock will emerge. The lining-rock interface behavior during the whole water-filling process can be illustrated as Fig. 3.

4.2 Friction-contact method (FCM)

The lining-rock interface behaviors in hydraulic pressure tunnels can be classified into contact mechanics problems and have been attached great importance for a long time (Salehnia 2015). In the conceptual point of view, the contact between two different pervious solids will definitely generate some restrictions in their displacements (Wriggers 2006, Wriggers and Zavarise 2004), which ensures the displacement continuity and flow continuity conditions at the lining-rock interface. After the detachment of lining-rock interface, the displacement restrictions are weakened or eliminated, indicating that the displacement continuity condition at the interface is no longer met. The point-to-point model, point-to-surface model and the surface-to-surface model are the three common contact

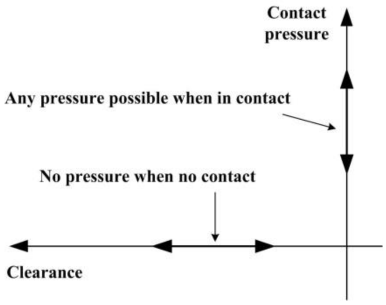

Fig. 4 Contact pressure-overclosure relationship

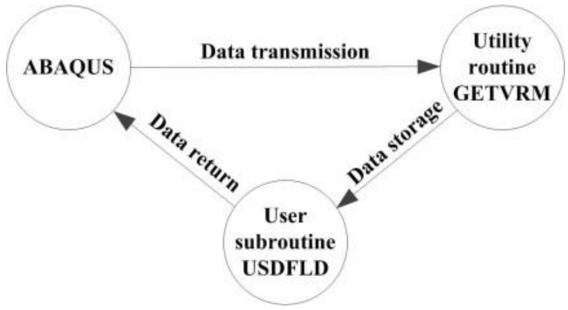

Fig. 5 Relationship among ABAQUS, GETVRM and USDFLD

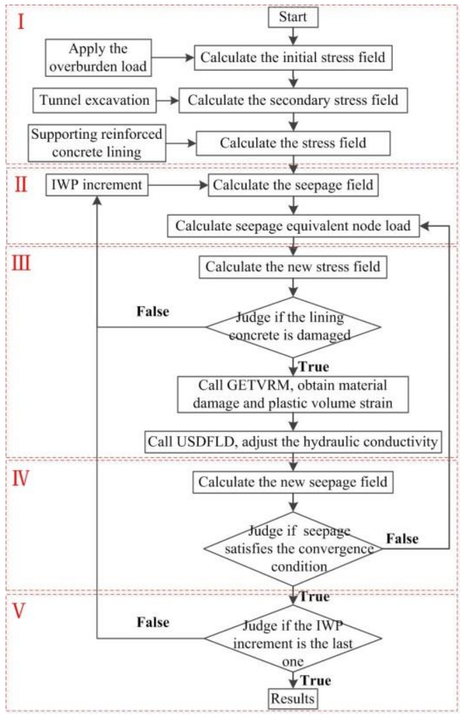

Fig. 6 Calculation process

models. Among them, the adopted surface-to-surface model distinguishes itself with its effectiveness in reducing the local stress concentration and contact pressure nonuniformity (Su *et al*. 2017, Zhang and Wu 2016).

In this study, the friction-contact method (FCM) is utilized to simulate the lining-rock interface behavior. Yan *et al*. (2018) adopted this modeling method to simulate the interaction between lining and surrounding ground, but the focus of their research work is on the stress transmission under close contact rather than the detachment of contact surfaces. The interaction between contact surfaces consists of two parts, namely the normal effect and the tangential effect. The detachment between lining and surrounding rock can be considered one kind of normal responses. The definition of normal behaviors in the contact pair is very clear, that is, only the compression state can pass the normal contact pressure. The tangential stress, or friction, can be passed only when the contact pair is in a sticking state. When the friction is less than the allowable value $\tau_{\max}$ (expressed as Eq. (22)), the contact pair is sticking. Once the friction exceeds $\tau_{\max}$, the relative sliding initiates.

$$\tau_{\max} = \mu p \tag{22}$$

where μ represents the friction coefficient, and p refers to the normal contact compressive stress.

In the calculation of stress field, the contact pair is mainly used to transmit mechanical responses at the lining-rock interface. While in the calculation of seepage field, the contact pair can ensure the infiltration of porous fluid between different pervious materials. Salehnia *et al*. (2017) proposed the hydro-mechanical interface element to simulate the lining-rock interface behavior, and the function of contact pair in this study is similar to that of hydro-mechanical interface element. The contact pressure-overclosure relationship can be illustrated in Fig. 4.

5. Implementation in ABAQUS

The seepage calculation and structural analysis of hydraulic pressure tunnel can be implemented in ABAQUS independently. However, the synchronous adjustment of hydraulic conductivity cannot be realized without the assist of utility routine GETVRM and user subroutine USDFLD. The function of GETVRM is accessing the material point information and that of USDFLD is defining field variables at material points as functions of any available data within GETVRM. In this study, the GETVRM is called to obtain the computational data of material damage and plastic volume strain from ABAQUS, the USDFLD is called to store these computational data as the form of state variables and define the hydraulic conductivity as a field variable, which is a comprehensive function of state variables. After this, the USDFLD returns the calculated field variable to ABAQUS so as to update the hydraulic conductivity. The relationship among ABAQUS, GETVRM and USDFLD can be illustrated as Fig. 5.

In order to ensure the computational efficiency and accuracy, the graded iterative method is adopted and the IWP is divided into three stages (Bian *et al*. 2009): (1) apply the critical IWP when the concrete damage initiates in one effort through the trial algorithm; (2) apply the IWP increment at a small value after the emergence of damage; (3) an appropriate increase in IWP increment is allowed after the appearance of macroscopic cracks. Specific calculation steps are proposed as follows (illustrated in Fig. 6).

(I) Apply the overburden load to simulate the initial stress field. Calculate the secondary stress field after the tunnel excavation. Finally, calculate the stress field after

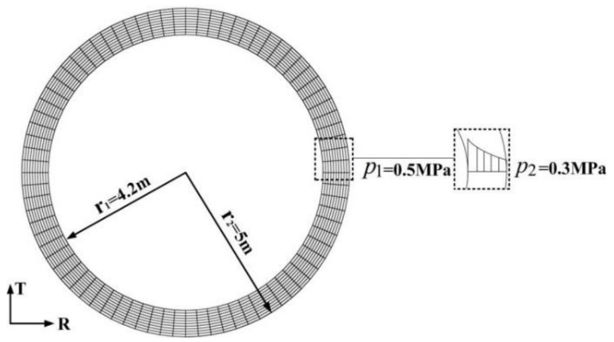

Fig. 7 Finite element model

supporting the lining and the cast-in-place reinforced concrete lining is assumed not to bear the excavation-induced load.

(Ⅱ) Calculate the seepage field after applying the IWP increment to the lining intrados, and calculate the seepage equivalent node load.

(Ⅲ) Apply the equivalent node load to the model nodes and calculate the structural stress, strain and damage. If the lining concrete is undamaged, apply the next IWP increment until damage occurs. If the lining concrete is damaged, adjust the hydraulic conductivity with USDFLD based on the computational data obtained by GETVRM.

(Ⅳ) Calculate the new seepage field with the secondary hydraulic conductivity, and check if the seepage field has reached a steady state with Eq. (23). If this criterion is satisfied, the steady seepage state is considered to have been reached. If not, calculate the equivalent node load again and repeat steps (Ⅲ) and (Ⅳ) until this criterion is satisfied.

$$\left|\frac{P_{n+1}-P_n}{P_n}\right| \le \delta \tag{23}$$

where P_{n+1} and P_n denote the seepage water pressures after n+1 and n iterations, δ refers to the iterative controlling threshold value. In this study, δ =1%.

(Ⅴ) Judge if the current IWP increment is the last one. If not, apply the next IWP increment and repeat steps (Ⅱ)-(Ⅳ) until the IWP reaches the maximum value.

6. Finite element modeling and analysis

6.1 Simplified example

The finite element model of a pervious thick-walled cylinder under inner water pressure p_1 = 0.5 and out water pressure p_2 = 0.3 MPa is established (see Fig. 7). The numerical model contains 1760 nodes and 800 elements. The inner radius r_1 = 4.2 m and outer radius r_2 = 5 m. The elastic modulus E = 28 GPa and Possion's ratio μ_c = 0.167. The hydraulic conductivity is taken as 1×10^{-9}m/s. In the numerical simulation, p_1 and p_2 are considered as the inner and outer pressure boundary conditions.

Schleiss (1986) assumed that the seepage water pressure is logarithmic distributed in the cylindrical zone. Neglecting the gravity, the hoop stress σ_θ and radial stress σ_r at arbitrary point can be estimated according to Eq. (24).

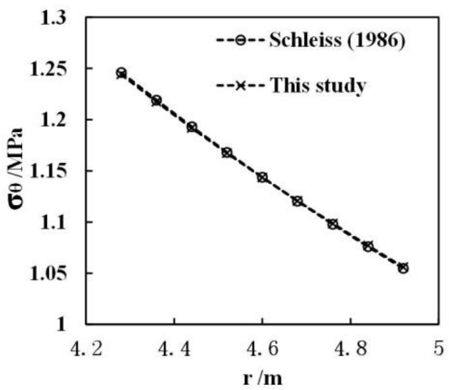

(a) Hoop stress

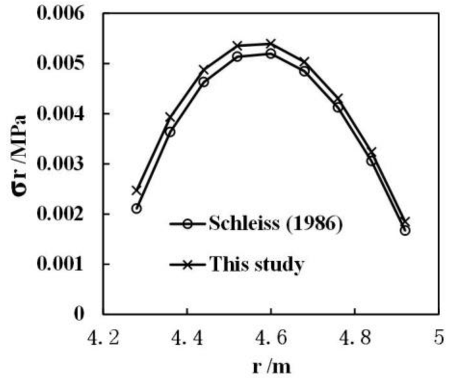

(b) Radial stress

Fig.8 Comparison of calculated results from Schleiss (1986) and this study

$$\begin{cases} \sigma_\theta = \dfrac{p_1-p_2}{2(1-\mu_c)}\cdot\left(\dfrac{1+(r_2/r)^2}{t^2-1}+\dfrac{\ln(r_2/r)+1-2\mu_c}{\ln t}\right) \\ \sigma_r = \dfrac{p_1-p_2}{2(1-\mu_c)}\cdot\left(\dfrac{1-(r_2/r)^2}{t^2-1}+\dfrac{\ln(r_2/r)}{\ln t}\right) \end{cases} \tag{24}$$

Based on Eqs. (15)-(17), the numerical solution of this study is implemented in ABAQUS, and the analytical solution is estimated according to Eq. (24). As illustrated in Fig. 8, the numerical solution of this study matches well with the analytical solution of Schleiss (1986), no matter in stress magnitude or stress distribution, which verifies the reliability of the proposed solution preliminarily.

6.2 Engineering numerical model

As shown in Fig. 9, the FCM model of a circular hydraulic pressure tunnel located in the shaft section is developed to analyze the cracking process of reinforced concrete lining and the involved hydro-mechanical interaction. The FCM model domain includes finite element models of reinforced concrete lining, surrounding rock and lining-rock interface. The radial model range is taken as 30 times of the excavation diameter D (D=10m) (Zhou *et al*. 2018), and the model range along the water-flow direction is taken as 10m. The inner and outer radii of lining are 4.2m and 5m respectively. The inner steel bars RB1 and the outer steel bars RB2 are embedded in the lining concrete. The distance from RB1 to the tunnel center is 4.3m, and

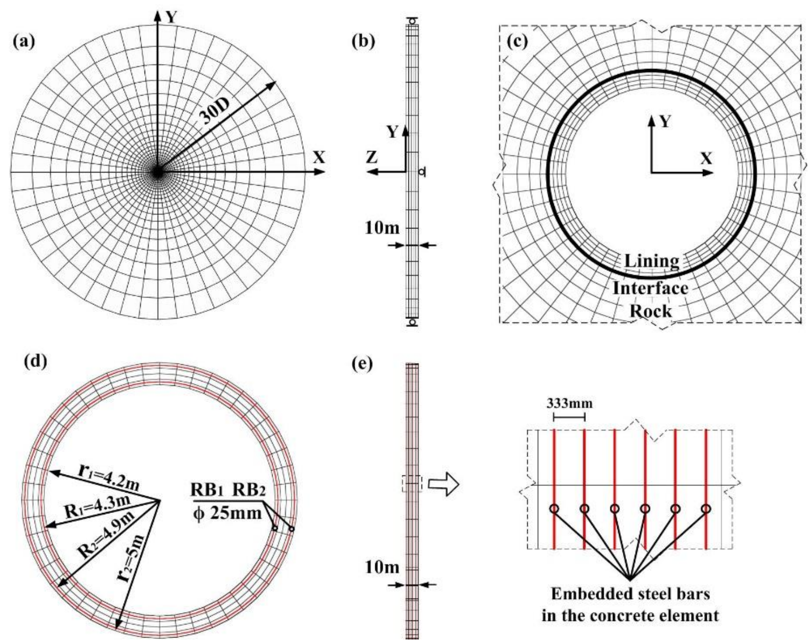

Fig. 9 FCM model: (a) whole model layout in the cross-section, (b) whole model profile along the water-flow direction, (c) details of lining-rock interface, (d) reinforced concrete lining model layout in the cross-section, (e) reinforced concrete lining profile and partial enlarged detail along the water-flow direction

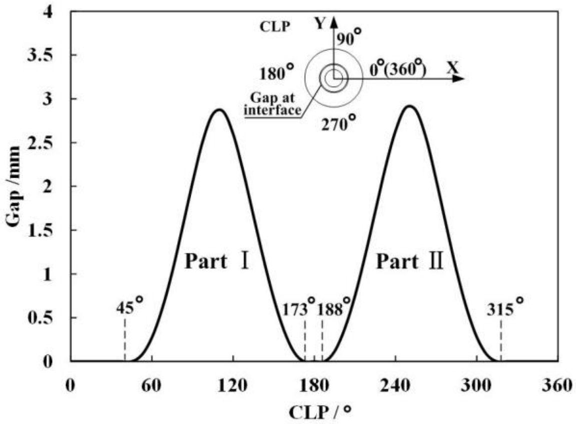

Fig. 10 Gap distribution at lining-rock interface along the CLP

that of RB2 is 4.9m. The diameter of steel bars is 25mm and the spacing between adjacent steel bars along the water-flow direction is 333mm. In this study, the lining concrete and the surrounding rock are simulated by C3D8P elements (8-node trilinear displacement and pore pressure elements with freedom degrees of displacements in x, y, z directions and pore pressure). The steel bars are modeled by T3D2 elements (2-node linear displacement truss element with freedom degrees of displacements in x, y, z directions) under the assumption that there is no relative slip between lining concrete and steel bars (ABAQUS 2011, Demir *et al*. 2016). The friction-contact elements are employed to connect the lining and the surrounding rock. There are 9865 nodes and 7888 elements in the model domain. The elastic moduli of surrounding rock, lining and steel bar are 8GPa, 28GPa and 206GPa respectively, and the Poisson's ratios are 0.25, 0.167 and 0.3 respectively. The hydraulic conductivities of rock mass and integral concrete are taken as 1×10^{-7}m/s and 1×10^{-9}m/s. The friction coefficient μ of the lining-rock interface is set to 0.5 (Zhou *et al*. 2018). The X axis and Y axis are both in the cross-section, and the Z axis is in the vertical plane with the right-hand rule satisfied. The origin of Cartesian coordinate system is located at the tunnel center.

6.3 Calculation conditions

In order to simulate the initial stress field, the upper surface of numerical model, where Z=0, is subjected to 100m-overburden-pressure caused by the upper rock mass. During the calculation process, the bottom surface of the model domain, where Z=-10m, is normally restrained in the displacement. Normal displacement restriction and zero head boundary condition are applied at the outer circumferential boundary of the surrounding rock. Changeable head boundary condition is set at the lining intrados to apply the IWP increment. In this study, the IWP is applied to the lining intrados from 0.4MPa to 0.81MPa with each IWP increment controlled within 0.001MPa-0.02MPa, and the gravity is neglected.

6.4 Simulation results

The reinforced concrete lining and surrounding rock are well-combined at the beginning of water-filling period, and the displacement continuity condition is met at the lining-rock interface. After the lining cracking, they are detached from each other gradually and the displacement continuity condition is no longer satisfied. Fig. 10 illustrates the gap distribution at the lining-rock interface at the end of water-filling period. A circular location path (CLP) whose origin is set at the right side of the tunnel is defined in the counterclockwise direction along the lining circumference.

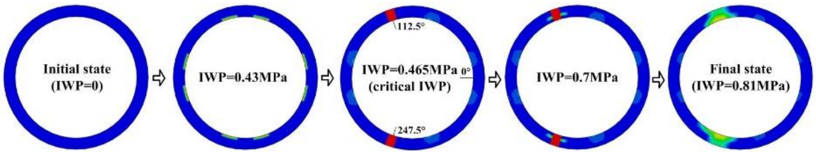

Fig. 11 Cracking characteristics of reinforced concrete lining

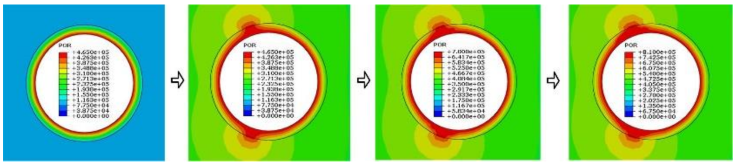

Fig. 12 Evolution characteristics of seepage field (POR refers to the seepage water pressure)

Table 1 Comparison between solutions of Schleiss (1986) and this study under the IWP of 0.4MPa

Item	Seepage water pressure on lining extrados /MPa	Hoop stress on lining extrados /MPa	Radial displacement on lining extrados /mm
Schleiss (1986)	0.0761	0.910	0.163
This study	0.0760	0.969	0.169
Error /%	0.0526	6.484	3.559

Table 2 Engineering practices of tunnel water-filling test

Test parameters	Engineering projects					Results in this study
	Yuzixi	Yuzixi	Hunanzhen	Xierhe	Chaersen	
Modulus of rock /GPa	5	3.0-3.6	11-16	8.1	1.5-5.0	8
Tunnel test length /m	15	14	35	33.7	28	10
Tunnel inner radius /m	2.5	2.5	4	2.4	3	4.2
Thickness of lining /m	0.5-0.6	0.1-0.15	0.2	0.12	0.1	0.8
Maximum IWP /MPa	1.2	0.78	1.365	0.57	0.5	0.81
Number of cracks	2	3	1	1	1	2

Table 3 IWP when cracks emerge in NSM and FCM models

Model	IWP when crack emerges /MPa						
	1st & 2nd	3rd	4th	5th	6th	7th	8th
NSM model	0.495	0.525	0.547	0.590	0.620	0.683	0.730
FCM model	0.465	-	-	-	-	-	-

The simulation results are mapped onto the CLP. As shown in Fig. 10, the gap distribution at the lining-rock interface exhibits good symmetry along the CLP. The detachment zone can be divided into two parts according to the crack distribution (Fig. 11). Part Ⅰ distributes from 45° to 173° and part Ⅱ distributes from 188° to 315° along the CLP. The detachment zone reaches 83% in total. Moreover, the gap widths at the 112.5° position and the 247.5° position, where macroscopic cracks locate, reach the maximum value of 2.9mm.

Within the elastic mechanics framework, Schleiss (1986) analyzed the structural responses of hydraulic pressure tunnel under the seepage body force. In order to validate the reliability of the proposed solution further, some calculated items from the proposed solution under the IWP of 0.4MPa are compared with those from Schleiss (1986) in Table 1. The minor errors of calculated results indicate the proposed solution is capable of simulating the structural responses of hydraulic pressure tunnel.

Fig. 11 presents the cracking characteristics of reinforced concrete lining in the FCM model. The lining cracks under the critical IWP of 0.465MPa, and two macroscopic cracks occur at 112.5° position and 247.5° position on the CLP. After this, no new cracks emerge and the damaged zone of the cracked site continues to expand with the IWP, indicating that the gap opening at the lining-rock interface can effectively inhibit the generation of new cracks. The reason for this phenomenon is that the surrounding rock bears most of the water load and the lining bears a small proportion after the detachment. Several large-scale water-filling tests of hydraulic pressure tunnels have been conducted in China (shown in Table 2), and the observed

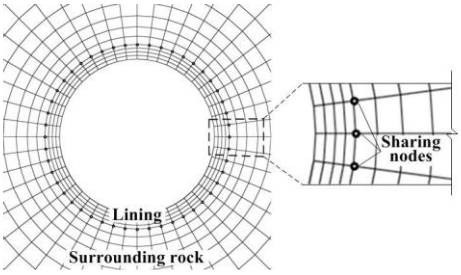

(a) NSM model

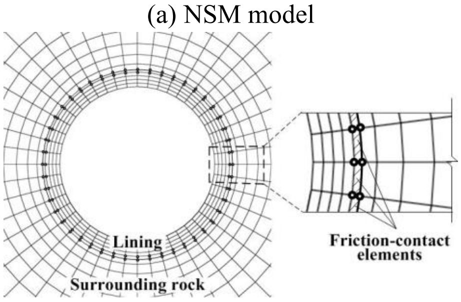

(b) FCM model

Fig.13 Difference between NSM model and FCM model

results in these field tests show the similar lining cracking characteristics. A few macroscopic cracks appear when the IWP is increased to the critical value, no new cracks emerge subsequently (Zhou *et al*. 2018). The cracking characteristics of reinforced concrete lining in the FCM model matches well with those in the water-filling tests. On one hand, this compatibility between simulation results and test results confirms the validity of employing friction-contact elements to model the lining-rock interface. On the other hand, it also implies thatthe lining was very likely to have been detached from the surrounding rock during the water-filling period in these field tests.

As illustrated in Fig. 12, the distribution of seepage field is changed significantly with the emergence of macroscopic cracks. Before the appearance of cracks, the reinforced concrete lining bears most of the water load and the seepage water pressure dwindles gradually from lining intrados to extrados. The seepage water pressure in the surrounding rock is relatively small due to the low-permeability of integral lining concrete. Macroscopic cracks appear when the IWP reaches the critical value, forming obvious leakage channels. The seepage water pressure at the cracked sites increases significantly, and consequently the hydraulic gradient decreases dramatically. The seepage water pressure gradually dissipates from the cracked sites to the deep of surrounding rock.

7. Discussions

In this section, the traditional NSM model is established, in which the lining and the rock mass are connected by sharing nodes under the assumption that the lining and the surrounding rock are well-combined during the whole water-filling period. The difference between NSM and FCM models only lies in the connection method between lining and surrounding rock (see Fig. 13). All the other conditions are the same, including material properties, loading conditions, boundary conditions, calculation process and so on. The obtained numerical results are comparatively analyzed with those in the FCM model.

Table 4 Maximum hydraulic conductivity of cracked lining concrete in NSM and FCM models

Model	Maximum hydraulic conductivity of cracked concrete /m/s	
	Initial state	Final state
NSM model	1×10^{-9}	1.35×10^{-6}
FCM model	1×10^{-9}	1.07×10^{-6}

In the NSM model, the displacement continuity condition at the lining-rock interface is satisfied all the time, and consequently there is no gap at the interface. As shown in Table 3, the cracking characteristics of reinforced concrete lining exhibit obvious inconsistency in NSM and FCM models. It can be found that there are eight macroscopic cracks at the end of water-filling process in the NSM model. Each macroscopic crack appears successively under different IWP except for the first two cracks. Under the critical IWP of 0.495MPa, the first two cracks appear at the same time. With the increase of IWP, other cracks emerge under IWPs of 0.525MPa, 0.547MPa, 0.59MPa, 0.62MPa, 0.683MPa and 0.73MPa respectively. The reason for this phenomenon is that the lining continues to deform outwardly in the radial direction with the surrounding rock, although the water load acting on the lining has been dramatically reduced due to the lining cracking. Compared with the NSM model, the number of macroscopic cracks can be significantly reduced in the FCM model, and the critical IWP for the first two cracks is reduced from 0.495MPa to 0.465MPa. This difference in simulation results indicates that the gap opening at the lining-rock interface can effectively inhibit the emergence of new cracks.

As the IWP increases, the damage initiates gradually on the reinforced concrete lining, leading to great improvement of permeability in the damaged zones. Table 4 presents the maximum hydraulic conductivity of cracked lining concrete. It can be found that the maximum decreases from 1.35×10^{-6} m/s to 1.07×10^{-6} m/s after the friction-contact element is introduced to model the lining-rock interface behavior, almost a decrease of 20.74%. This change indicates that the detachment between lining and surrounding rock can slow down the damage evolution of lining to some degree.

The steel bar RB1 is taken to analyze the evolution characteristics of reinforcement stress at the cracked sites. Fig. 14 illustrates the reinforcement stresses at the cracked sites in FCM and NSM models under different IWPs. Before the lining cracking, the reinforcement stresses increase with the IWP, and the reinforcement stress is roughly proportional to the IWP whether in the FCM model or the NSM model. In the FCM model, the reinforcement stress at the cracked site experiences a sharp rise due to the stress release of concrete cracking under the critical IWP of 0.465MPa. As the IWP continues to increase, the growth rate of the reinforcement stress obviously slows down and a significant phenomenon of stress retraction occurs. When the IWP reaches the maximum, the reinforcement stress at the cracked site is only 40.685MPa. In the NSM model, the crack emerges when the IWP reaches the critical pressure of

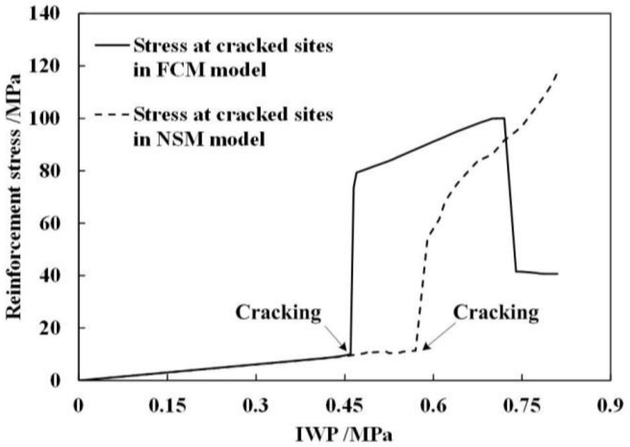

Fig. 14 Evolution characteristics of reinforcement stresses at cracked sites in FCM and NSM models

0.590MPa (the 5th crack in Table 3), the reinforcement stress in the cracked site keeps rising with the IWP and the maximum reinforcement stress reaches about 117.414MPa at the end of water-filling period. From observation of the reinforcement stresses at the cracked sites in FCM and NSM models, it can be found that the stress evolution shows significant differences, which is caused by theintroduction of friction-contact element to simulate the lining-rock interface behavior. In the NSM model, the lining and the surrounding rock are connected by sharing nodes, they will not be detached from each other and the lining continuously expands outward in the radial direction, resulting in the sustainable growth of reinforcement stress at the cracked sites. However, in the FCM model, the inner water exosmosis caused by the lining cracking and the restraints of embedded reinforcements lead to the gradual detachment between lining and surrounding rock. The reinforced concrete lining bears a small proportion of the water load and the outward deformation is obviously weakened or even eliminated. Therefore, the growth rate of the reinforcement stress obviously slows down and the phenomenon of stress retraction arises. The evolution characteristics of reinforcement stress and the stress values in the FCM model explain the observed results of relevant engineering projects well (Zhou *et al*. 2015).

Some previous research work has been done to investigate the evolution characteristics of reinforcement stress at the cracked sites, such as Schleiss's analytical solution (Schleiss 1997) and Zareifard's analytical solution (Zareifard 2018). The reinforcement stress from the former solution increases zigzag with the IWP and that from the latter solution increases approximately linearly with the IWP. However, after the lining cracking, the reinforcement stress in the FCM model increases approximately linearly with the IWP and finally falls back to a small value. Some differences can be found in the evolution characteristics of reinforcement stress among these three solutions because they were solved under different assumptions and methodologies. The detachment between lining and surrounding rock has been taken into account in the FCM model, which results in the phenomenon of reinforcement stress retraction.

8. Conclusions

The reinforced concrete lining in hydraulic pressure tunnels will crack under a certain IWP, and the inner water leaks off along cracks, manifesting typical hydro-mechanical interaction.

- The indirect-coupled method between hydraulic mechanics and structural mechanics is employed to reflect the coupling effects. The mechanical effect of seepage field is expressed as the equivalent node load obtained by the seepage body force, and the secondary hydraulic conductivity of concrete lining is evaluated according to the material damage and the plastic volume strain with the adoption of utility routine GETVRM and user subroutine USDFLD in the finite element code ABAQUS.
- The friction-contact method (FCM) is introduced to simulate the lining-rock interface behavior. In the FCM model, the cracking process of reinforced concrete lining shows good consistency with that in water-filling tests of engineering practices. Compared with the traditional NSM model, the FCM model can effectively reduce the number of cracks and slow down the damage evolution of reinforced concrete lining. Moreover, the evolution characteristics of reinforcement stresses match well with the observed results in engineering practices.

Acknowledgments

The research described in this paper was financially supported by the National Key Research and Development Program of China [grant number 2016YFC0401803]; the National Natural Science Foundation of China [grant number 51579194, 51879207].

References

ABAQUS (2011), "User's Manual", Version 6.11. Dassault Systemes.

Bian, K., Liu, J., Xiao, M., and Liu, Z. (2016), "Cause investigation and verification of lining cracking of bifurcation tunnel at Huizhou Pumped Storage Power Station", *Tunnel. Underground Space Technol.*, **54**(27), 123-134. https://doi.org/10.1016/j.tust.2015.10.030.

Bian, K., Xiao, M., and Chen, J. (2009), "Study on coupled seepage and stress fields in the concrete lining of the underground pipe with high water pressure", *Tunnel. Underground Space Technol.*, **24**(3), 287-295. https://doi.org/10.1016/j.tust.2008.10.003.

Bobet, A., and Nam, S. W. (2007), "Stresses around pressure tunnels with semi-permeable liners", *Rock Mech. Rock Eng.*, **40**(3), 287-315. https://doi.org/10.1007/s00603-006-0123-6.

Cicekli, U., Voyiadjis, G. Z., and Al-Rub, R. K. A. (2007), "A plasticity and anisotropic damage model for plain concrete", *J. Plasticity*, **23**(10-11), 1874-1900. https://doi.org/10.1016/j.ijplas.2007.03.006.

Dadashi, E., Noorzad, A., Shahriar, K., and Goshtasbi, K. (2017), "Hydro-mechanical interaction analysis of reinforced concrete lining in pressure tunnels", *Tunnel. Underground Space Technol.*, **69**, 125-132. https://doi.org/10.1016/j.tust.2017.06.006.

Dadashi, E., Noorzad, A., Shahriar, K., and Goshtasbi, K. (2018), "An optimal method to design reinforced concrete lining of pressure tunnels", *J Mining Environ.*, **9**(4), 829-837.

Demir, A., Caglar, N., Ozturk, H., and Sumer, Y. (2016), "Nonlinear finite element study on the improvement of shear capacity in reinforced concrete T-Section beams by an alternative diagonal shear reinforcement", *Eng. Struct.*, **120**, 158-165. https://doi.org/10.1016/j.engstruct.2016.04.029.

Fahimifar, A., and Zareifard, M. R. (2009), "A theoretical solution for analysis of tunnels below groundwater considering the hydraulic–mechanical coupling", *Tunnel. Underground Space Technol.*, **24**(6), 634-646. https://doi.org/10.1016/j.tust.2009.06.002.

Fahimifar, A., and Zareifard, M. R. (2013), "A new closed-form solution for analysis of unlined pressure tunnels under seepage forces", *J. Numeric. Anal. Method. Geomech.*, **37**(11), 1591-1613. https://doi.org/10.1002/nag.2101.

Fernández, G. (1994), "Behavior of pressure tunnels and guidelines for liner design", *J. Geotechn. Eng.*, **120**(10), 1768-1791. https://doi.org/10.1061/(ASCE)0733-9410(1994)120:10(1768).

Grassl, P., and Jirásek, M. (2006), "Damage-plastic model for concrete failure", *J. Solid. Struct.*, **43**(22-23), 7166-7196. https://doi.org/10.1016/j.ijsolstr.2006.06.032.

Graziani, A., and Boldini, D. (2012), "Influence of hydro-mechanical coupling on tunnel response in clays", *J. Geotech. Geoenviron. Eng.* **138**(3), 415-418. https://doi.org/10.1061/(ASCE)GT.1943-5606.0000597.

Hou, J. (2009), "Observed data analysis of water filling test of the high-pressure tunnel in Tianhuangping Pumped-Storage Power Station", *Adv. Sci. Technol. Water Resource.***29**(2), 27-31.

Jaeger, C., (1979), *Rock Mechanics and Engineering*, Second ed., Cambridge University Press, London, England.

Jankowiak, T., and Lodygowski, T. (2005), "Identification of parameters of concrete damage plasticity constitutive model", *Foundation. Civil. Environ. Eng.*, **6**, 53-69.

Lee, J., and Fenves, G. L. (1998), "Plastic-damage model for cyclic loading of concrete structures", *J. Eng. Mech.*, **124**(8), 892-900. https://doi.org/10.1061/(ASCE)0733-9399(1998)124:8(892).

Leung, C., and Meguid, M. A. (2011), "An experimental study of the effect of local contact loss on the earth pressure distribution on existing tunnel linings", *Tunnel. Underground Space Technol.*, **26**(1), 139-145. https://doi.org/10.1016/j.tust.2010.08.003.

Lubliner, J., Oliver, J., Oller, S., and Onate, E. (1989), "A plastic-damage model for concrete", *J. Solid. Struct.*, **25**(3), 299-326. https://doi.org/10.1016/0020-7683(89)90050-4.

Lyu, D., Yu, C., Ma, S., and Wang, X. (2018), "Nonlinear seismic response of a hydraulic tunnel considering fluid-solid coupling", *Math. Problem. Eng.*, **2018**, 1-12. https://doi.org/10.1155/2018/9608542.

Mazars, J., and Pijaudier Cabot, G. (1989), "Continuum damage theory-application to concrete", *J. Eng. Mech.*, **115**(2), 345-365. https://doi.org/10.1061/(ASCE)0733-9399(1989)115:2(345).

MOHURD, (2010), Code for design of concrete structure GB50010-2010; China Architecture & Building Press, Beijing, China.

Olumide, B. A. (2013), "Numerical coupling of stress and seepage in the design of pressure tunnel under to high internal water pressure", *J. Eng. Technol.*, **3**(3), 235-244.

Olumide, B. A., and Marence, M. (2012), "A finite element model for optimum design of plain concrete pressure tunnels under high internal pressure", *J. Eng. Technol.*, **1**(5), 235-244.

Picandet, V., Khelidj, A., and Bellegou, H. (2009), "Crack effects on gas and water permeability of concretes", *Cement Concrete Res.*, **39**(6), 537-547. https://doi.org/10.1016/j.cemconres.2009.03.009.

Rama, J. S. K., Chauhan, D. R., Sivakumar, M. V. N., Vasan, A., and Murthy, A. R. (2017), "Fracture properties of concrete using damaged plasticity model -a parametric study", *Struct. Eng. Mech.*, **64**(1), 59-69. https://doi.org/10.12989/sem.2017.64.1.059.

Salehnia, F., (2015). "From some obscurity to clarity in Boom Clay behavior: Analysis of its coupled hydro-mechanical response in the presence of strain localization", Ph.D Dissertation, Universite´ de Lie`ge, Liege.

Salehnia, F., Sillen, X., Li, X. L., and Charlier, R. (2017), "Numerical simulation of a discontinuous gallery lining's behavior, and its interaction with rock", *J. Numeric. Anal. Method. Geomech.*, **41**, 15691589. https://doi.org/10.1002/nag.2689.

Schleiss, A. J. (1986), "Design of pervious pressure tunnels", *Water Power Dam Constr.*, **5**, 21-26.

Schleiss, A. J. (1997), "Design of reinforced concrete linings of pressure tunnels and shafts", *Int. J. Hydropow. Dams*, **4**(3), 88-94.

Shin, J. H. (2008), "Numerical modeling of coupled structural and hydraulic interactions in tunnel linings", *Struct. Eng. Mech.*, **29**(1), 1-16. https://doi.org/10.12989/sem.2008.29.1.001.

Shin, J., Kim, S., and Shin, Y. (2012), "Long-term mechanical and hydraulic interaction and leakage evaluation of segmented tunnels", *Soils and Foundations*, **52**(1), 38-48. https://doi.org/10.1016/j.sandf.2012.01.011.

Simanjuntak, T. D. Y. F., Marence, M., Mynett, A. E., and Schleiss, A. J. (2013), "Mechanical-hydraulic interaction in the lining cracking process of pressure tunnels", *Int. J. Hydropow. Dams*, **20**(5), 98-105.

Su, K., Yang, Z., Zhang, W., Wu, H., Zhang, Q., and Wu, H. (2017), "Bearing mechanism of composite structure with reinforced concrete and steel liner: An application in penstock", *Eng. Struct.*, **141**, 344-355. https://doi.org/10.1016/j.engstruct.2017.03.021.

Wriggers, P., (2006), *Computational Contact Mechanics*, Springer, Germany.

Wriggers, P., and Zavarise, G., (2004), *Computational Contac Mechanics*, Encyclopedia of Computational Mechanics, Wiley, New Jersey, USA.

Xiao, M., and Zhao, C. (2017), "Stability Analysis of Steel Lining at Pressure Diversion Tunnel Collapse Zone during Operating Period", *Math. Problem. Eng.*, **2017**, 1-14. https://doi.org/10.1155/2017/3280414.

Xue, W., Yao, Z., Jing, W., Tang, B., Kong, G., and Wu, H. (2019), "Experimental study on permeability evolution during deformation and failure of shaft lining concrete", *Construct. Build. Mater.*, **195**, 564-573. https://doi.org/10.1016/j.conbuildmat.2018.11.101.

Yan, Q., Li, B., Deng, Z., and Li, B. (2018), "Dynamic responses of shield tunnel structures with and without secondary lining upon impact by a derailed train", *Struct. Eng. Mech.*, **65**(6), 741-750. https://doi.org/10.12989/sem.2018.65.6.741.

Yoo, C. (2005), "Interaction between Tunneling and Groundwater-Numerical Investigation Using Three Dimensional Stress-Pore Pressure Coupled Analysis", *J. Geotech. Geoenviron. Eng.* **131**(2), 240-250. https://doi.org/10.1061/(ASCE)1090-0241(2005)131:2(240).

Yoon, J., Han, J., Joo, E., and Shin, J. (2014), "Effects of Tunnel Shapes in Structural and Hydraulic Interaction", *KSCE J. Civil Eng.*, **18**(3), 735-774. https://doi.org/10.1007/s12205-014-1325-1.

Zareifard, M. R. (2018), "An analytical solution for design of pressure tunnels considering seepage loads", *Applied Mathematical Modelling*, **62**, 62-85. https://doi.org/10.1016/j.apm.2018.05.032.

Zareifard, M. R., and Fahimifar, A. (2016), "A simplified solution for stresses around lined pressure tunnels considering non-radial symmetrical seepage flow", *KSCE J. Civil Eng.*, **20**(7), 2640-2654. https://doi.org/10.1007/s12205-016-0105-5.

Zhang, Q., and Wu, H. (2016), "Sliding behaviour of steel liners on surrounding concrete in c-cross-sections of spiral case structures", *Struct. Eng. International*, 333-340. https://doi.org/10.2749/101686616X14676302920032.

Zhang, W., Dai, B., Liu, Z., and Zhou, C. (2018), "Numerical algorithm of reinforced concrete lining cracking process for pressure tunnels", *Eng. Comput.*, **35**(1), 91-107. https://doi.org/10.1108/EC-11-2016-0394.

Zhou, L., Su, K., Zhou, Y., Wen, X., and Wu, H. (2018), "Hydro-mechanical coupling analysis of pervious lining in high pressure hydraulic tunnel", *J. Hydraulic Eng.*, **49**(3), 313-322.

Zhou, Y., Su, K., and Wu, H. (2015), "Hydro-mechanical interaction analysis of high pressure hydraulic tunnel", *Tunnel. Underground Space Technol.*, **47**, 28-34. https://doi.org/10.1016/j.tust.2014.12.004.

CC